X-644-72-162

PREPRINT

NASA TM X- 65953

MAGNETIC COERCIVITY AND FERROMAGNETIC SPECIES IN LUNAR MATERIALS

PETER WASILEWSKI

JUNE 1972

GSFC

GODDARD SPACE FLIGHT CENTER

GREENBELT, MARYLAND

43P

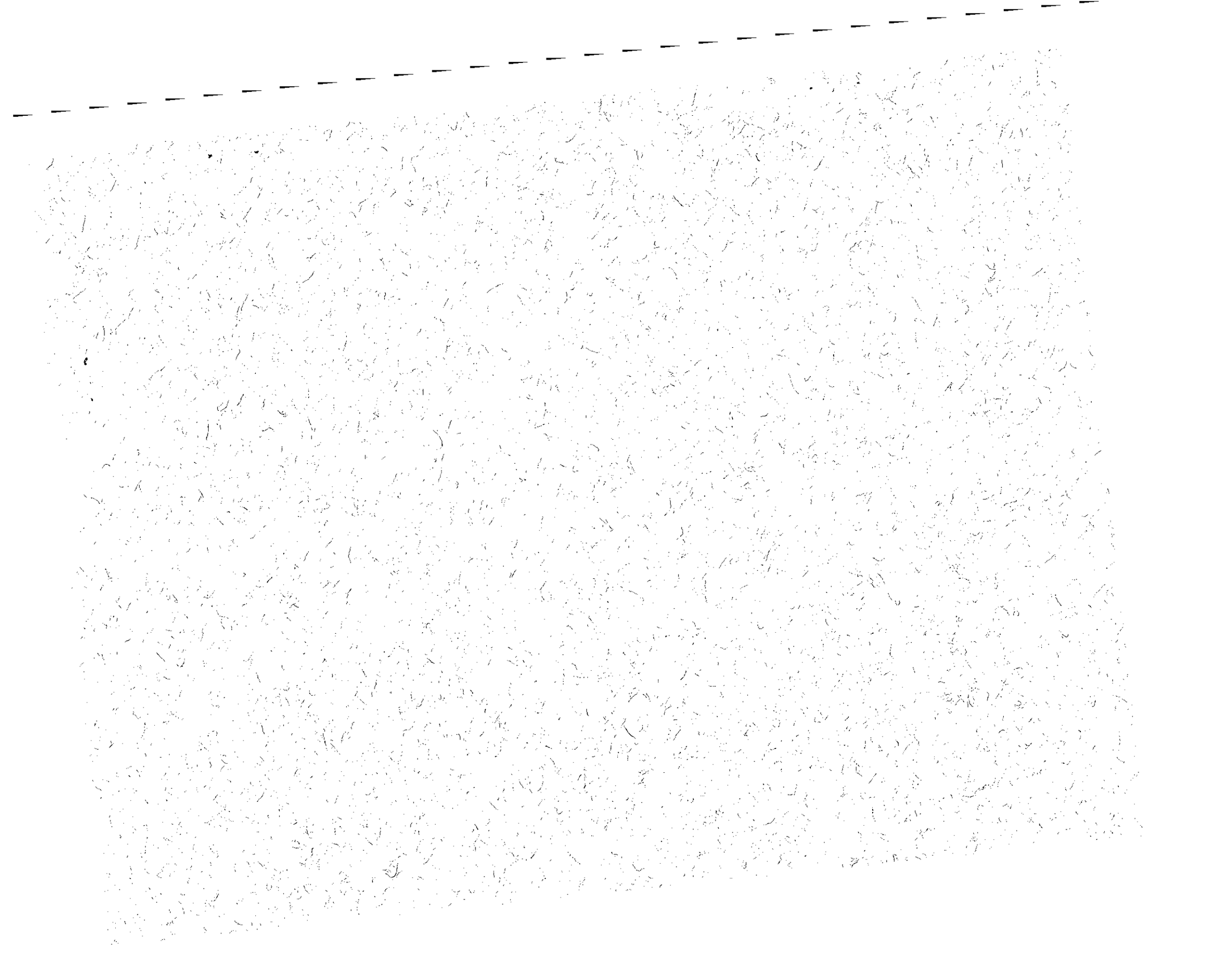

Magnetic Coercivity and Ferromagnetic Species in Lunar Materials

Peter Wasilewski*

Planetology Branch
Goddard Space Flight Center
Greenbelt, Maryland 20771

*Research Associate Professor at George Washington University, Washington, D. C.

Abstract:

Lunar samples have reduced coercive force (H_c), high values of R_H (ratio of remanent coercive force, H_R, to coercive force, H_c), and constriction in their magnetic hysteresis loops due to the presence of superparamagnetic and multidomain iron grains. These results are consistent with the observed size distribution of metal in the lunar samples. The high R_H values are also attributable to the magnetic shape effects of the iron grains. Spheres, cubes, and needles, as well as more irregular metal grains have been observed. The coercive force values normally considered to represent magnetic hardness are quite meaningless unless the size and shape distributions are determined. The R_H and R_I (ratio of saturation remanence to saturation magnetization) values can be considered characteristic of the size and shape modes of the ferromagnetic grains in a natural sample, and a classification of natural materials based on their magnetic hysteresis characteristics is presented with special reference to lunar samples.

Introduction:

Lunar crystalline rocks contain iron and troilite, often found in eutectic intergrowth, ulvospinel, chrome-spinels, ilmenite, and other iron-bearing phases. It is quite conceivable that the ordering of impurity cations in troilite and other iron-bearing phases may render them ferromagnetic. The lunar fines contain all of the minerals found in the crystalline rocks, as well as glass components containing metallic spherules, meteoritic debris, metallic splatter, and platelet coating due to deposition of vaporized impact material.

Iron configurations which are easily observed with an optical "microscope" or scanning electron microscope are shown diagramatically in Figure 1A. These iron configurations are found in the crystalline rocks, in microbreccia samples, and as coating on the lunar fines and rocks. In Table 1 a listing of the different classes of Fe found in lunar samples is considered from a genetic viewpoint. The observed size range of iron and the magnetic effects due to size, shape, and composition are also listed in Table 1.

In ascertaining what Fe-bearing species are responsible for the ferromagnetic properties of lunar materials, magnetic powder analysis should be utilized (Wasilewski, 1972a) to determine shether the presence of cation substitution in FeS and the various spinels renders them ferro-

magnetic. This technique is nondestructive and yields information which cannot be acquired by means of conventional reflected light microscopy.

The distribution of iron in lunar assemblages ranges from iron dissolved in glass (paramagnetic iron) to free iron in the size range < 100 Å (superparamagnetic) to millimeter (multidomain) sizes. Constriction in the magnetic hysteresis loops for lunar samples is observed and high values of the ratio, R_H (remanent coercive force, H_R, to coercive force, H_c) are obtained (Wasilewski, 1972b, c). The constriction is easily explained as due to the presence of discrete mixtures of superparamagnetic, single domain and multidomain components (Wasilewski, 1972b). The particle shape distribution is also important in explaining the R_H values. The main distinctions between lunar, terrestrial, and meteoritic materials are presented in this paper based mainly on properties of the magnetic hysteresis loops.

Metallic Particles:

Ferromagnetic species exist in lunar samples in three size categories: (a) superparamagnetic (<100 Å), (b) single domain ($\sim$200-1000 Å), and (c) multidomain (several μm or larger). Superparamagnetic particles are so small that the magnetic anisotropy energy is less than or approximately the same as the thermal fluctuation energy at the measuring temperature. Therefore, the

magnetization is randomly affected by thermal activation, and these particles exhibit a "pseudoparamagnetic" behavior (superparamagnetism) with large moments. Single domain particles are large enough so that they are thermally stable at measuring temperature with magnetization determined by the anisotropy energy minimum and particle properties. Multidomain particles are so large that magnetization in low fields occurs by domain wall motion. Superparamagnetic particles have zero coercive force and no hysteresis, the multidomain particles have low coercivity and hysteresis, and single domain particles have high coercive force. Accepting that all three size categories of metallic species exist in lunar material, a supposition which is probably quite correct for all lunar samples, then the magnetization behavior must be considered in terms of mixtures of the three categories.

Particle Shape and Size:

Bean and Jacobs (1960) examined the magnetization curve of a dilute suspension of multidomain iron powder (spheres). The experimentally determined saturation field was 6000 $\pm$ 200 Oe. in good agreement with the theoretical value, ($4\pi/3I_S$ 1-F = 6150 $\pm$ 300), with F, the volume fraction of ferromagnetic material. Any metal sphere has a demagnetization factor N = $4\pi/3$ so that the resultant field, H, inside the sphere is given by H = H_a-NI_S, where H_a is the applied field, and I_S the satura-

tion magnetization. The spherical shape is responsible for the apparent magnetic hardness in some samples and gives rise to the high H_R values.

Senftle, et al. (1964) have reported a field and temperature independent susceptibility at fields 6000 Oe. for small metallic spheres in tektites at which point saturation was achieved and the susceptibility is zero. To examine lunar materials high fields are required and the characteristic properties of spheres must be considered in an interpretation. For single domain or multidomain spheres the same conditions hold, and if the sphere is polycrystalline, deviations can be expected due to internal stress and individual crystallite orientations.

Magnetization Curves Due to Mixtures:

Since we are obviously concerned with mixtures of Fe particles covering a broad range of sizes, and since the lunar fines and breccia samples contain glasses with high iron content, it is important to evaluate nondestructive methods of magnetic analysis which can yield information about the relative concentration, size, and shape of Fe species. Magnetization curves can be used for this purpose. In Figure 2a magnetization curves for a paramagnetic, a ferromagnetic, and a mixture of both species are shown. Curve I is for a small amount of contained ferromagnetic impurity and Curve II is a typical curve for a paramagnetic. These curves can be considered to represent,

for example, the expected situation for lunar samples. Curve III is the composition of Curves I and II. The effect of the ferromagnetic impurity is best evaluated by extrapolation to H=0. At this point I/v is the saturation magnetization per unit volume of the mixture, from which the amount of ferromagnetic impurity (Curve I) can be evaluated. The shape field (H_S) can be evaluated as well (see Figure 2b). Figure 2b is an illustration of the magnetization curve for a dilute suspension of multidomain single crystal iron spheres (after Bean and Jacobs, 1960). The divisions in the magnetization process are predicted on the basis of the demagnetization factor for a sphere, the volume fraction of ferromagnetic material present, and in the case of polycrystalline spheres the orientation of individual crystals with respect to the field. Evaluation of approach to saturation using I vs. H^{-1} or H^{-2} plots reveals sharp changes in slope at fields of about 7000 Oe. for the iron spheres. The approach laws apparently do not apply for fields below 7000 Oe. In the lunar samples the approach laws cannot be effectively applied above or below 7000 Oe. unless corrections are made because of the shape effect as well as because of the influence of superparamagnetism, and a significant paramagnetism.

Hysteresis Loops (Experimental Results):

Magnetic hysteresis loops for terrestrial and extra-

terrestrial natural materials have been measured on a vibrating sample magnetometer in fields to 16 K. Oe. Hysteresis loops are presented in Figures 3, 4, 5, and 6.

Natural materials are dilute dispersions of ferromagnetic phases in a non-magnetic matrix, and in most cases the dispersion is such that the phases may be considered as irregular shaped and non-interacting. An added feature in impactites, lunar materials, and tektites is the presence of spherical-shaped ferromagnetic phases and superparamagnetism. Depending on the amount of spherules and and superparamagnetism, the magnetization curves will be modified accordingly.

In most terrestrial samples the field needed for magnetic saturation is low and the magnetic hysteresis loop parameters depend on the grain size distribution, composition, and degree and extent of thermochemical alteration (Wasilewski, 1969, 1970, 1972). Illustrated in Figure 3 are hysteresis loops for samples (a) M01-a single crystal of Fe_3O_4 containing numerous hematite lamellae; (b) Diorite (798); (c) 557-a continental basalt which was formerly a magnetic class I (Wasilewski, 1968, 1969) sample, but which has been altered by heating in air for 60 hours at 600° C., 850° C. for sintering, then annealed at 500° C; and (d) a synthetic sample (X=0.6) of titanomagnetite before and after heating. The external field for saturation is quite low, of the order of three

thousand Oersted at most for terrestrial samples. The hysteresis increases from M01 to 557 along with coercivity and remanence.

In contrast to the opps in Figure 3 we present the loops for lunar fines (10084-89) and breccia (10021) (Figure 4) (Nagata et al., 1970, 1971). The most striking feature of these loops is the linear increase in magnetization with increase in applied field at high fields. This is due to significant "paramagnetism." Comparing the fines and breccia powder, another observation of importance is the point at which the magnetization curve departs from the linear aspect of the magnetization loop. For the breccia powder this occurs at about 2 K. Oe., while for the fines this occurs at about 8 K. Oe. The interpretation for this observation is simply that superparamagnetism and spherical shaped ferromagnetic phases are relatively more significant in the fines. Subtracting the paramagnetism from the breccia (10021) loop results in a saturation at $\sim$ 2 K. Oe., while for the fines this is reached at $\sim$ 8 K. Oe., as can be seen in the figure.

The constriction in the low field region of the hysteresis loops for breccia powder (10021), fines (10084), and breccia (10085) is shown in Figure 5. The constriction and reduced coercivity are due to the effect of mixing components. The effect of adding superparamagnetic

components of zero H_c and multidomain components of low H_c along with their high effective magnetization in low fields results in high H_R/H_c values and constriction. Hysteresis loop parameters for lunar samples, chondrites, steel spheres (52100) and impactites (Monturaqui) are listed in Table I.

Figure 6 illustrates hysteresis loops for a polycrystalline steel sphere, the Forest City Bronzite chondrite (H5-Van Schmus and Wood, 1967), and the Allende carbanaceous chondrite (Clarke et al., 1970). Alloy additions in the FeNi system, along with the chemical gradients and particle shape, will all cause complications in evaluation of the magnetization curves, particularly the approach to saturation and behavior in the low field region. The effects of shock and Ni content are presently being evaluated, so that quantitative analyses of chondrites and iron meteorites can be made.

Shape Fields:

The aspect of the magnetization curves which is important in evaluating initially the role of shape anisotropy is the field H_S mentioned earlier in the discussion of lunar fines and breccia. This may be best understood by reference to Figure 6 which illustrates curves for the sphere and the chondrites. The field H_S is that field which marks departure of the curve from linearity and is directly related to particle shape (i.e., the

shape demagnetizing factor). This field varies for different materials, and for a specific shape is dependent on saturation magnetization (I_S). For example, the saturation field H_S for a sphere of iron ($4\pi/3 \cdot I_S$) is about 3.5 times that for a magnetite sphere. Examining a curve such as illustrated for the lunar fines (Figure 4) immediately produces the interpretation that (a) high I_S phases are present and (b) high shape demagnetizing fields are involved. There is no way in which a terrestrial sample, except for rare samples which do contain iron, can have a curve resembling the lunar fines.

Reduced Coercivity:

Any rock can be considered as a dilute mixture of ferromagnetic particles of irregular shape with a distribution of grain sizes dispersed in a nonmagnetic silicate matrix in such a manner that magnetic interactions between grains may be neglected. Since it is fairly well established that Fe is ubiquitous and of variable mode of origin, producing particles ranging in size from superparamagnetic to multidomain, it is necessary to evaluate the effect of this broad range of Fe particles ($\sim$100 Å to $\sim$ 1 mm) on the coercivity.

Superparamagnetic particles have $H_c=0$; single domain particles have $H_c=10^3-10^4$, depending on the anisotropy, and the H_c of multidomain particles is of the order of

10. Thus we can consider the treatment of Kneller and Luborsky (1963) who defined the H_c of superparamagnetic (SP) and multidomain (MD) species to be equal to zero.

The coercivity of a mixture ($\bar{H}_c$) of SD and either SP or MD particles is then $\bar{H}_c = H_c(1 + H_c q/I_R \; \epsilon / 1-\epsilon)^{-1}$, where H_c=coercivity of SD particles, $I_R = I_R(\infty)$, $q=(NM_S)^{-1}$ for MD, $q=(VM_S/3KT)$ for SP particles, and ϵ equals concentration of SP or MD particles (see Kneller and Luborsky, 1963). In Figure 7a a series of curves relating $\bar{H}_c/H_c$ to the concentration of zero coercivity particles with $H_c \cdot q/I_R$ as the parameter. These curves are in good agreement with the data of Meikeljohn (1953) (see Figure 7b). From the figure it can be seen that the SP particles reduce the coercive force more than MD particles for the same concentration. This is in agreement with the fact that MD particles will have a finite distribution of coercivities and different magnetization curves compared to SP particles.

Luborsky and Lawrence (1961) measured the saturation magnetization of iron particles < 100 Å in diameter. Extremely high fields were necessary to saturate the samples at 300° K. Even at 76° K. fields of > 50 K. Oe. were necessary to unambiguously determine the saturation magnetization. The maximum H_c for Fe occurs at a particle diameter of ~ 130 Å (Luborsky and Paine, 1960). From electron microscope observations (R. M. Fuller, private

communication) and consideration of the general mode of formation of spherules of iron in impactites, and the further added aspect of high vacuum deposition (low PO_2) in a lunar environment and where particles of glass and rock may fall through an aerosol of vaporized material, it is clear that a complete range of particle sizes from superparamagnetic to multidomain are found in the lunar material. Thus the hysteresis behavior, including observed constriction, can be explained on the basis of the particle sizes and shapes of high I_S material of varying mode of origin.

Coercivity Ratio ($R_H=H_R/H_C$):

For a random assembly of uniaxial particles reversing magnetization by coherent rotation, the value of $R_H=1.094$ (Wohlfarth, 1958). For planar or spherically random assemblies of independent, identical, uniaxial particles reversing magnetization by coherent rotation, curling, or fanning the ratio R_H lies between 1.0 and 1.2 (Luborsky and Morelock, 1964). Variations in this ratio can be accounted for by considering the effect of the distribution of critical fields. Gaunt (1960) calculated a maximum $R_H=2.02$, assuming a broad rectangular distribution of critical fields.

Values of R_H greater than the predicted values can be obtained by (a) a significant zero coercivity superparamagnetic component and (b) a multidomain component.

Values of R_H greater than 10 have been obtained by Lothian *et al.* (1958) in Cu-Co alloys and is ascribed to superparamagnetism. This can be understood by reference to our previous consideration of reduced coercivity due to the presence of SP and MD components (Figure 7).

H_R is related to the critical field H_0 at which a discontinuous change in the direction of magnetization occurs, but this argument may not apply to bulk material. Bate (1961) also demonstrated that the maximum H_R and minimum H_c occurred in a measurement perpendicular to the direction of alignment in partially aligned γFe_2O_3 particles. In evaluating the magnetic properties of a precipitation alloy (Gold-Cobalt) Gaunt (1960) found the particle anisotropy distribution to be important in determining the ratio R_H. However, his calculations are a modification of the Stoner-Wohlfarth (1948) calculations, and, as mentioned, a maximum value of 2.02 is predicted. He does, however, make reference to the work of Lothian *et al.* (1958), who obtained R_H values $\gg 10$ for Cu-Co alloys. The explanation for the high values is in the significance of a superparamagnetic contribution which affects H but not H_R.

The effect of mixing components on R_H and the relative insignificance of coercive force as a parameter is clearly indicated in the data listed in Table II. The presence of shape anisotropy, particularly the presence

of spheres of high I_S material, will also have an extreme influence on the R_H value. For all samples in Table II, i.e., basalt, diorite, lunar microbreccia (MB), and a precipitation alloy, the coercive force (H_c) is 125 Oe., but as can be seen, the H_R values vary from 200 Oe. to 900 Oe. and the R_H value from 1.6 to 7.2. It is also clear that as R_H increases, R_I decreases. The range in hysteresis parameters for terrestrial and lunar materials is listed in Table III.

Effective anisotropy and the physical characteristics of the particle mixtures are most important in explaining the R_H value:

a. superparamagnetic phases
b. exchange anisotropy
c. multidomain phases
d. shock induced anisotropy
e. particle shapes
f. saturation magnetization of the phases.

Constriction in Hysteresis Loops:

To simulate the presence of variable coercivity mixtures (Wasilewski, 1970, 1971)in igneous rocks, two discs, A and B, were assembled and measured as a cylinder after being measured independently. Results of the measurements are illustrated in Figure 8, and information on the two discs is listed in Table IV. In Table IV $I_M(a)/I_M(b)=3.7$ and $H_c(a)/H_c(b)=0.12$. Thus, if A is a

component with $H_c=H_{cA}$, and B is a component with $H=H_{cB}$, where $H_{cA}<H_{cB}$, it has been demonstrated (Wasilewski, 1970, 1971) that

$$H_R/H_c(A+B) > H_R/H_c(A) > H_R/H_c(B).$$

If discrete mixtures are present, loop constriction is observed. The R_H variation with grain size in magnetite was first demonstrated by Parry (1965) who showed that the ratio R_H for large grains is greater than R_H for small grains.

Concerning the values of H_R and H_c for igneous rocks, another contribution due to the anisotropic rhombohedral decomposition products must be considered. This consideration is not applicable in the case of lunar samples, since the R_H data for the ilmenite-hematite series is explained in terms of the Fe_2O_3 content (Wasilewski, 1970).

Relationships for All Natural Materials:

There are basic differences between lunar, terrestrial, and meteoritic samples, as well as differences within each of the above natural groups. These differences are manifest in the hysteresis properties of the samples. Figures 9 and 10 illustrate plots of H_c vs. H_R and R_I vs. R_H respectively. In these diagrams the distinctions between lunar and terrestrial rocks are clarly made. In the H_c vs. H_R plot (Figure 9) lines are drawn which correspond to specific R_H values. The terrestrial basalts lie in the range $1.2<R_H<2.0$, the diorites in the region 2.0

$R_H < 4.0$, and lunar materials $R_H > 4.0$. With the exception of Calliham, all chondrites have R_H values > 10.0. The samples with H_c=125 Oe. (Table II) fall on the dotted line in Figure 9. Explanation of the varying R_H values for samples of constant H_c (=125 Oe.) lies in the grain size and shape distributions of discrete components. More accurately, the real explanation resides in consideration of the effective coercivity distributions, but to delimit each effective distribution requires more detailed experimental work. A magnetization curve for a natural material can be considered as made up of four effective components, each of which has a discrete response to an applied field.

$$vf'(H)=v_{SD}f(H)+v_{SP}f(H)+v_{MD}f(H)+I/H$$

where v=the volume fraction and f(H)=the magnetization response for specific components to H. Subscript SD=single domain, SP=superparamagnetic, MD=multidomain, and I/H is the paramagnetic component. Each component, if discrete, has its own curve, and if present as a mixture, it should be easily evaluated, but in practice the particle size distributions are not single valued, and grain shape would complex any interpretation, even if the volume of different shaped particles were constant. In Figure 10 the values R_I vs. R_H are plotted, and this plot locates the various types of natural materials based on hysteresis loop data.

Much theoretical work has been devoted to the R_H

value (see reviews by Wohlfarth, 1963, and Kneller, 1969). According to the Stoner-Wohlfarth model (1948), the R_H value should be 1.094 (Wohlfarth, 1958); while for a rectangular anisotropy distribution applied to Gold-Cobalt precipitation alloys, the maximum R_H value is 2.02 (Gaunt, 1958). The natural samples which fall in the region $1.0 < R_H < 2.0$ are basaltic rocks (Wasilewski, 1972). Coarser grained terrestrial samples, such as diorites fall in the range $2.0 < R_H < 5.0$, the lunar samples have $R_H >$ 5.0, and the chondrites have R_H values > 10.0, with the exception of carbonaceous chondrites and those which are highly altered. The R_I values within the region $1.0 < R_H < 2.0$ range from 0.25 to 0.80, while for $R_H > 2.0$ the R_I values range from $\sim$ 0.2 down to 0.0005. There are essentially three regions which can be defined based on R_I and R_H values. The one contains the basaltic rocks, the second the diorites and granites, and the third, lunar samples and chondrites.

The microscopic coercivity spectrum is associated with an anisotropy spectrum, and it is necessary to relate the coercivity to a grain shape spectrum as well to completely evaluate R_H. The coercivity spectrum depends on the grain size, state of strain, chemical homogeneity, and grain shape. If interactions are important, the R_H value will also be influenced (Wohlfarth, 1963).

Discussion:

In highly reducing environment it is expected that discrete iron particles of extremely small dimensions would be distributed in a glass of high iron content. In fact, as Shaw and Heasley (1967) pointed out, superparamagnetic Fe_2O_3 and ferrites can form in repidly cooled silicate melts. Metallic iron particles ranging from $\sim$100 Å to millimeter size dimensions are expected and, indeed, are identified (Nagata, et al., 1970). Also, because of the wide range of particle sizes it may be somewhat difficult to precisely evaluate the superparamagnetism by techniques such as the classical H/T superposition principle. The existence of superparamagnetism is not uniquely defined by the R_H values such as have been measured for the lunar samples. Simulation with terrestrial rocks demonstrates that hysteresis loop constriction and high R_H values can be achieved by mixtures of discrete high and low coercivity components. The theoretical explanation of Kneller and Luborsky (1963), who consider the manner in which the coercivity is reduced in mixtures of single domain with superparamagnetic or multidomain particles, is invoked to explain the high R_H values and the constriction in lunar materials.

Another feature of magnetization experiments on lunar samples and impactites in general concerns the spherical shape of the metallic particles. At fields

less than about 7000 Oe. the spherical particle has an internal field $4\pi/3\ I_S$ such that the particle will show field independence at low fields. In all chondrites and in lunar samples the approach to saturation is a more complex phenomenon because of the presence of Fe and FeNi and the corresponding effect due to spheres and other shapes in materials of high saturation magnetization.

Conclusions:

1. All hysteresis loops for lunar materials have reduced H_c and high R_H values as a consequence of discrete individual components in a mixture of ferromagnetic components.

2. The loop constriction in the lunar samples is a consequence of the presence of discrete components of high, low, and zero coercivity in the mixture.

3. Superparamagnetism reduces H_c more than multidomain material for equivalent fractions of material.

4. Terrestrial basalts (magnetic Class I) have R_I values ranging from 0.25 to 0.80, R_H values ranging from $\sim$1.4 to 2.0, while lunar materials have R_I values $\geq$ 0.1 and R_H values $\geq$ 5.0. Chondrites have R_I values $<$ 0.1 and R_H values $>$ 10.0 (carbonaceous chondrites and most fines excluded).

5. Lunar samples compare favorably with precipitation alloys in their R_I and R_H values except that an added strong paramagnetic aspect is present in lunar samples.

6. Simple magnetic property analysis of lunar samples enables one to quickly evaluate the types and distributions of various components.

7. We have simulated the conditions which can produce the R_I and R_H values in terrestrial and lunar materials and qualitatively can assess the contributions of various components in producing loop constriction, reduced coercivity, and variable R_H and R_I values.

9. A sufficient theoretical basis has been previously established to explain the reduced coercivity due to mixtures.

10. The presence of spherical particles of high saturation magnetization in impactites, chondrites, and lunar samples requires high measuring fields ($H_A > 7000$) to properly evaluate the samples.

11. Magnetic analysis utilizing hysteresis curves allows one to separate the various components in a natural assemblage based on the shape of particles.

12. The series of samples with constant H_c but different H_R values clearly demonstrates that H_c is neither a critical field nor is it a useful parameter when comparing different types of natural materials which contain dispersions of ferromagnetic particles.

ACKNOWLEDGEMENTS

This work was done during the summer of 1971 while the author held an ASEE-NASA Summer Faculty Fellowship. Thanks are extended to Dr. Emad and Dr. Morakis for their assistance during the program tenure.

Thanks are also extended to Dr. French and Dr. Walter of the Planetology Branch for their assistance and for providing a stimulating environment to conduct research.

TABLE I

Summary of (a) classes of metal in lunar rocks and fines based on mode of origin (b) size range of metal particles in lunar materials and (c) magnetic effects due to variations in size, shape, and composition of metal in lunar rocks.

(a) Mode of Origin of Metal

Class I - primary crystallization
Class II - subsolidus reduction of spinels
Class III - shock melting
Class IV - vapor deposition

(b) Size Range of Metal

Optical microscopy	-	0.5 μm to 1000 μm
Scanning electron microscopy	-	0.05 μm to 5 μm
Electron microscopy	-	10 Å, 100 Å

(c) Magnetic Effects

1. Size:
SUPERPARAMAGNETISM-ambient temperature relaxation effects-temperature dependent blocking temperature effects over the lunar cycle 100° K. to 400° K.-zero coercivity-reduces coercivity and R_H in a mixture
MULTIDOMAIN-low coercivity-reduces coercivity and R_H in a mixture-time dependent magnetization acquisition in weak fields-source of noise in lunar samples
SINGLE DOMAIN-high magnetic stability-high coercive force-spectrum variable over the lunar temperature cycle 100° K. to 400° K.
2. Shape:
Spheres $<$ 0.05 μm to 100 μm; cubes $<$ 1 μm to 5 μm; needle shapes with length:diameter ratio $>$ 10:1; magnetostatically interacting chains of spheres and platelets
The shape fields $H_S=NI_S$ change resulting in discrete discontinuities in the magnetization curves.
3. Composition:
FeNiCo variation: Co - 0 to 8%; Ni - 0 to 40%.
Temperature dependent magnetization anomalies-Curie point variations-variable shock remagnetization mechanisms

TABLE II

Coercivity values for lunar samples, chondrites, steel sphere, and Monturaqui impactite.

Sample	H_C(Oe.)	H_R(Oe.)	R_H	R_I
Lunar				
12053-47	8	80	10	.004
12070-102	22	450	20.5	.05
10021-32	24	410	17.1	--
10084-89	36	460	12.8	.07
10048-55	50	520	10.4	.07
10085-16	125	670	5.4	0.16
Chondrites				
Forest City	10	400	40	--
Beenham	25	700	28	.03
Modoc	75	1100	14.6	.03
Calliham	165	270	1.6	.27
Others				
Steel sphere	50	800	16	--
Monturaqui	90	225	2.5	.07

TABLE III

Samples with constant H_C values but variable H_R values.

Sample	H_C	H_R	R_H	R_I
Basalt	125	200	1.6	.36
Diorite	120	500	4.1	.10
Lunar MB	125	675	5.4	.15
1% Co-Cu	125	900	7.2	.06

TABLE IV

Range of coercivity values for terrestrial and lunar materials.

	Terrestrial Material		Lunar Material	
	min.	max.	min.	max.
H_C	45	420	8	125
H_R	140	720	80	670
R_H	1.3	5.8	5.4	20.5
R_I	0.01	0.80	.004	0.16

TABLE V

	A(Soft)	B(Hard)	A+B
I_R/I_M	30.27	0.79	0.26
H_c(Oe.)	50	420	75

FIGURE CAPTIONS

Figure 1 - Examples taken from numerous studies in Proceedings of Apollo 11 and 12 Lunar Science Conferences to demonstrate the shape, distribution, and mode of origin of iron in lunar samples. (In the figure iron is black.)

Figure 2A- Magnetization curves for various discrete components which may exist in a natural sample.

Figure 2B- Magnetization curve for a mixture of polycrystalline iron spheres (after Bean and Jacobs, 1960).

Figure 3 - Hysteresis loops for natural terrestrial samples and synthetic titanomagnetite.
A. Single crystal magnetite - MO1
B. Diorite - 798
C. Basalt - 557A
D. Synthetic titanomagnetite ($xFe_2TiO_4 \cdot 1\text{-}xFe_3O_4$) x=0.6 before and after heating.

Figure 4 - Magnetic hysteresis loops for lunar fines (10084) and breccia (10021). The breccia sample is decomposed into ferromagnetic and paramagnetic components.

Figure 5 - Portion of low field region of hysteresis loops for lunar samples: breccia (10021), fines (10084), and breccia (10085), to illustrate the characteristic loop construction observed in lunar samples.

Figure 6 - Magnetic hysteresis loops for (a) polycrystalline steel sphere, (b) Forest City chondrite, and (c) Allende chondrite.

Figure 7 - Experimental and theoretical curves to support the proposition that mixing superparamagnetic (SP) and multidomain (MD) material with single domain (SD) material will reduce coercivity in the lunar samples.
A. Experimental results (Meikeljohn, 1953)
B. Theoretical curves (Kneller and Luborsky, 1963) ($H_c \cdot q/I_R$=1.0 for SD+MD and 3.2 for SD+SP.)

Figure 8 - Experimental simulation of reduced coercivity and loop construction due to mixtures. Samples 557 and CH21-001 have discrete size modes; the mixture is bimodal.

Figure 9 - Relationship between coercive force (H_C) and remanent coercive force (H_R) for natural materials.

Figure 10- Relationship between R_I and R_H, the hysteresis ratios. R_I is the ratio of remanent magnetization (I_R) to saturation magnetization (I_S), and R_H is the ratio of remanent coercive force (H_R) to coercive force (H_C).

FIGURE 1

IRON and IRON ALLOY (Ni + Co) – LUNAR

IRON SPHERULES IN GLASS

CROSS SECTION OF METAL LUMPS AT SURFACE OF GLASS AND SILICATES

AGGREGATE OF METAL DROPLETS ON SURFACE OF GLASS AND SILICATES

SMALL METAL CUBES IN GLASS

NETWORK CHAINS ON THE SURFACE OF SOIL PARTICLES

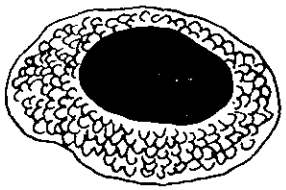

MOUND OF IRON SULFIDE SPHERULES WITH CENTRAL METAL CORE

IRON NEEDLES IN PYROXENE

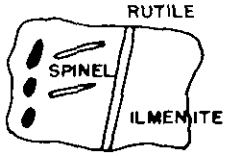

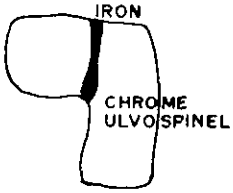

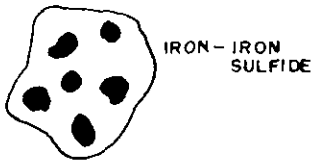

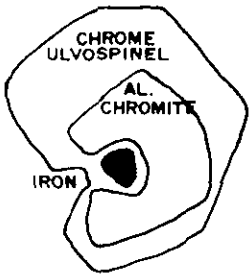

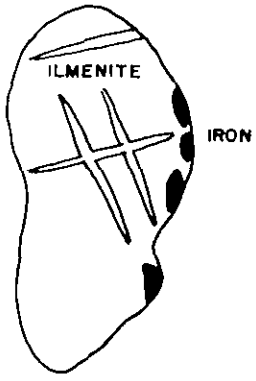

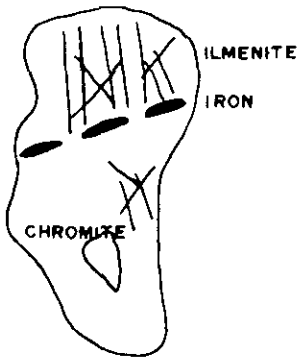

PRIMARY, SUBSOLIDUS, and EUTECTIC METAL

FIGURE 2A

MAGNETIZATION CURVES FOR VARIOUS HYPOTHETICAL ASSEMBLAGES

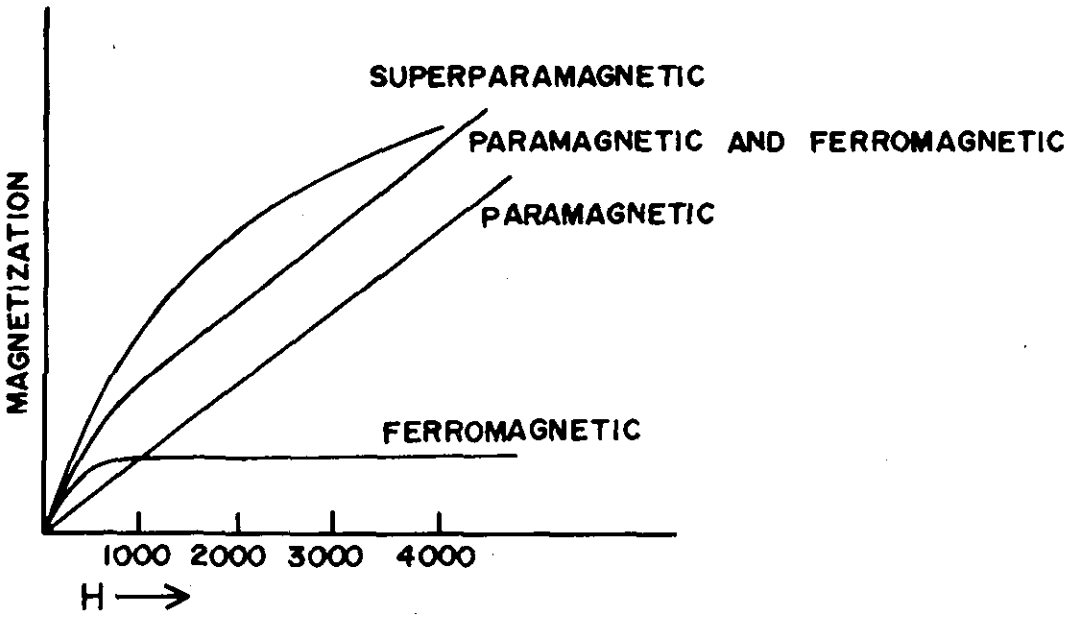

FIGURE 2B

MAGNETIZATION CURVE FOR A MIXTURE OF SMALL POLYCRYSTALLINE IRON SPHERES.

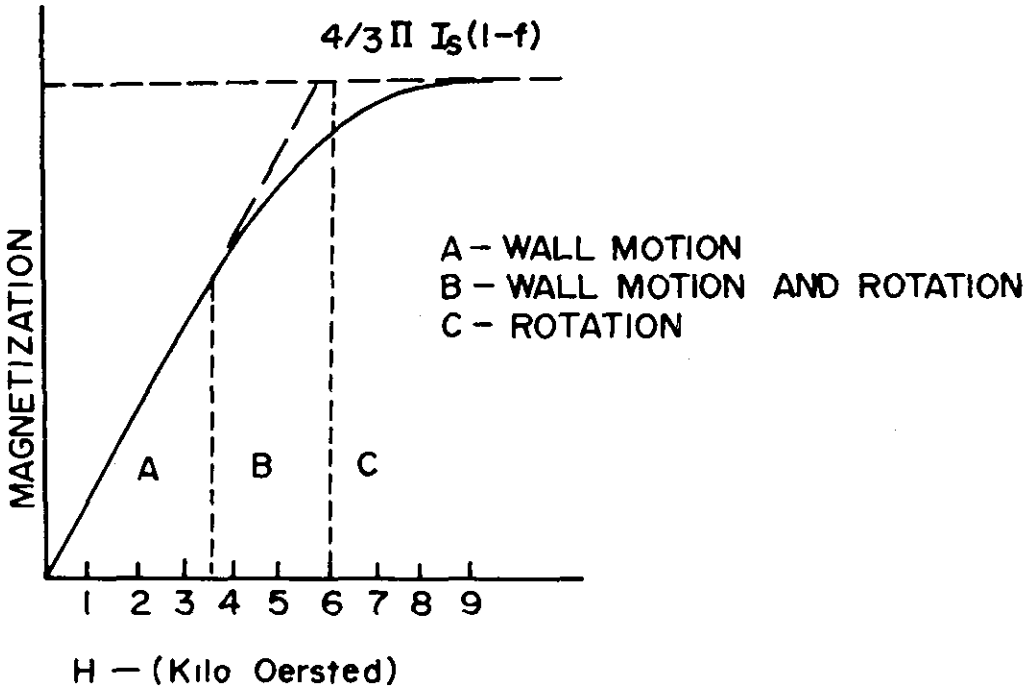

FIGURE 3

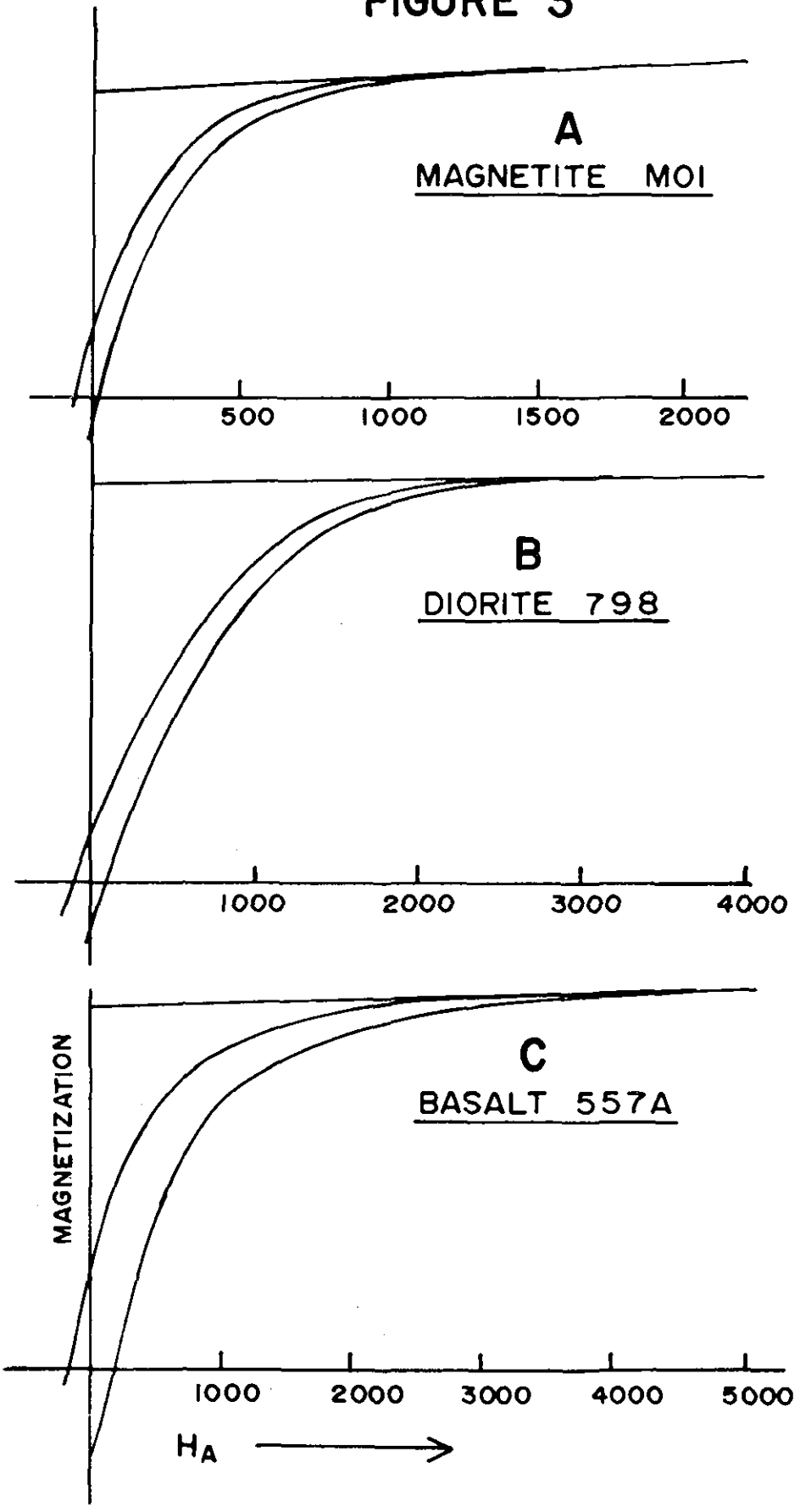
A
MAGNETITE MOI
500
1000
1500
2000
B
DIORITE 798
1000
2000
3000
4000
C
BASALT 557A
MAGNETIZATION
1000
2000
3000
4000
5000
H_A

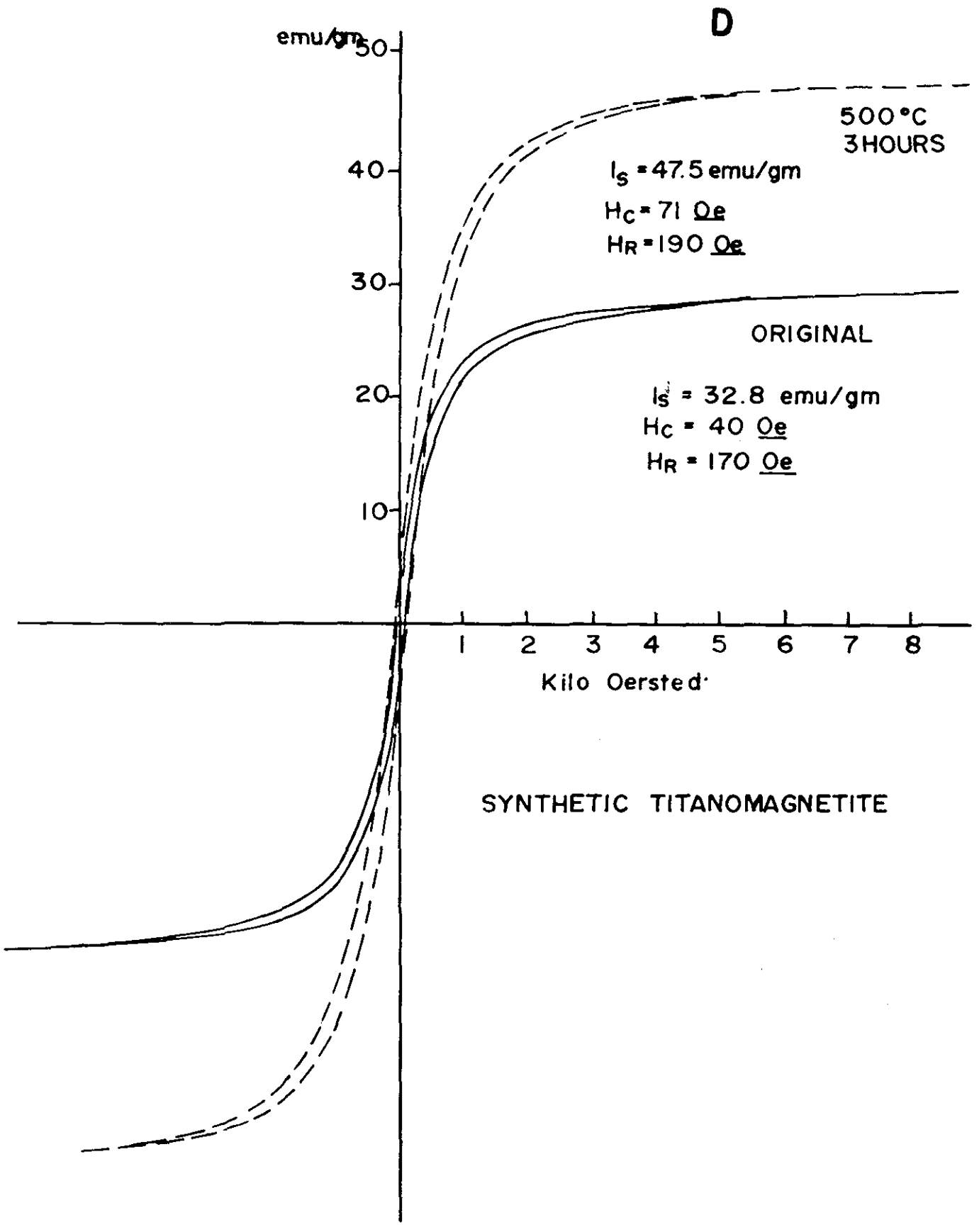
D
emu/gm
50
40
30
20
10
500°C
3HOURS
I_S = 47.5 emu/gm
H_C = 71 Oe
H_R = 190 Oe
ORIGINAL
I_S = 32.8 emu/gm
H_C = 40 Oe
H_R = 170 Oe
1
2
3
4
5
6
7
8
Kilo Oersted
SYNTHETIC TITANOMAGNETITE

FIGURE 4

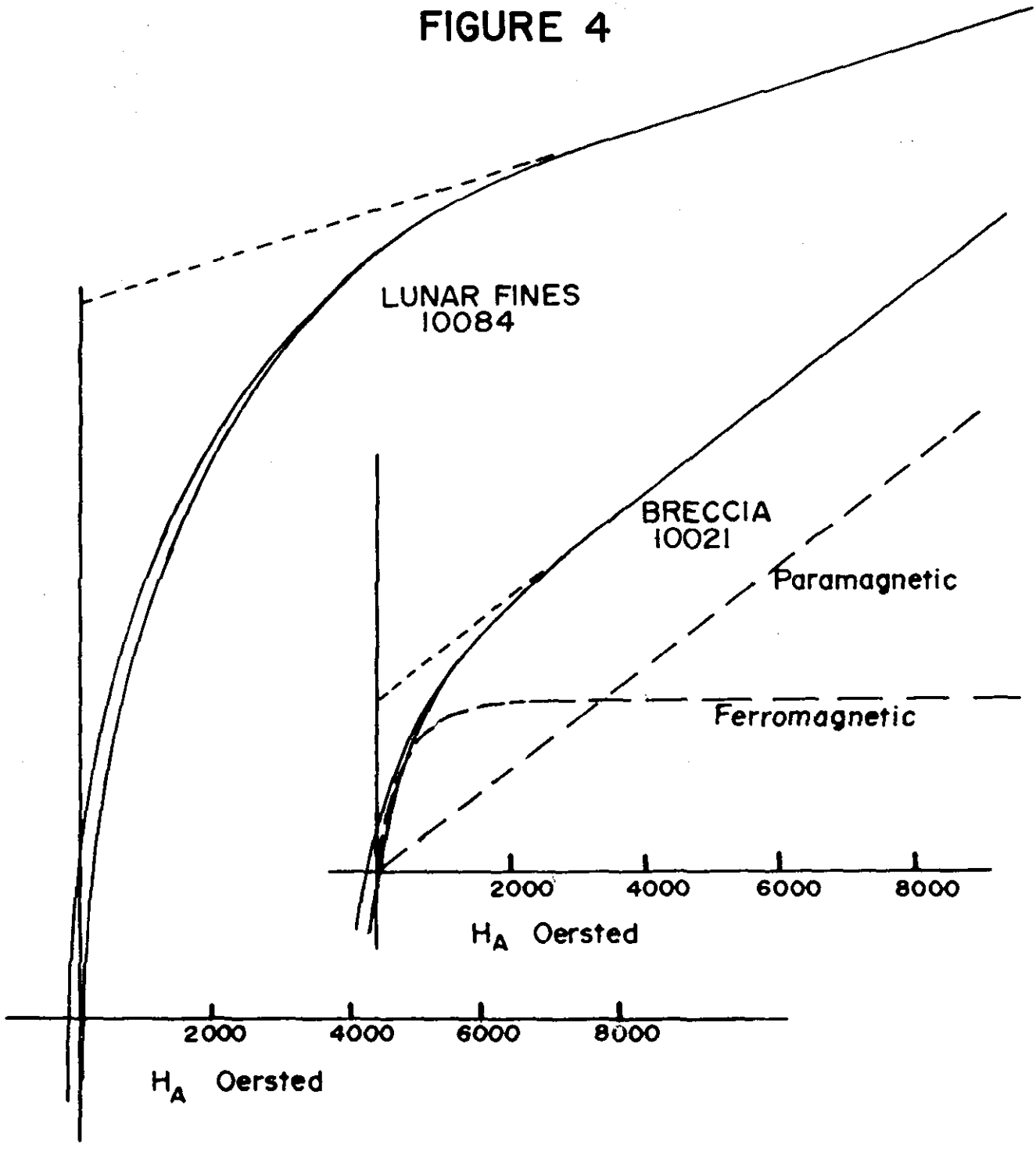
LUNAR FINES
10084
BRECCIA
10021
Paramagnetic
Ferromagnetic
2000
4000
6000
8000
H_A Oersted
2000
4000
6000
8000
H_A Oersted

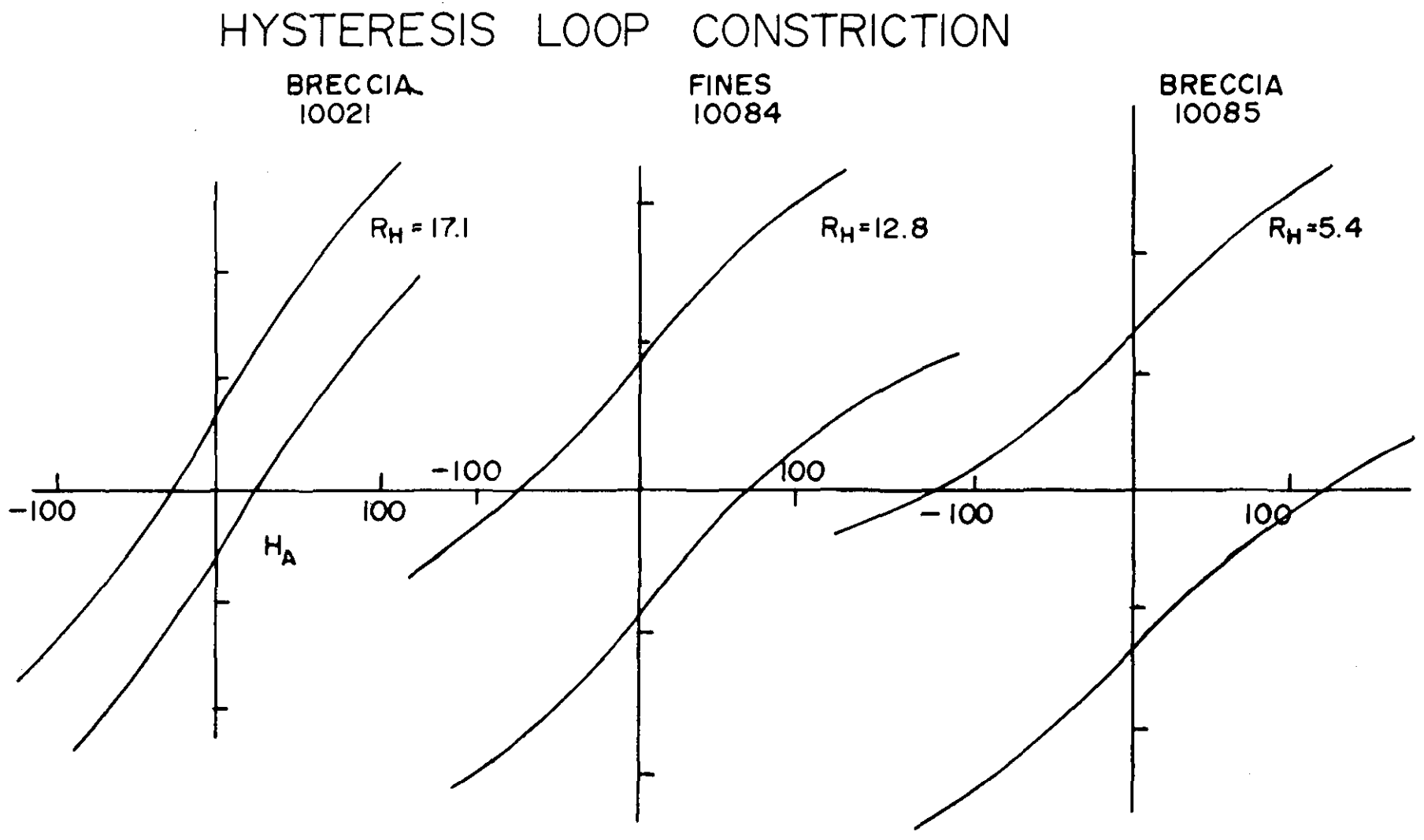
HYSTERESIS LOOP CONSTRICTION
BRECCIA
10021
FINES
10084
BRECCIA
10085
R_H = 17.1
R_H = 12.8
R_H = 5.4
-100
100
-100
100
-100
100
H_A

FIGURE 5

FIGURE 6

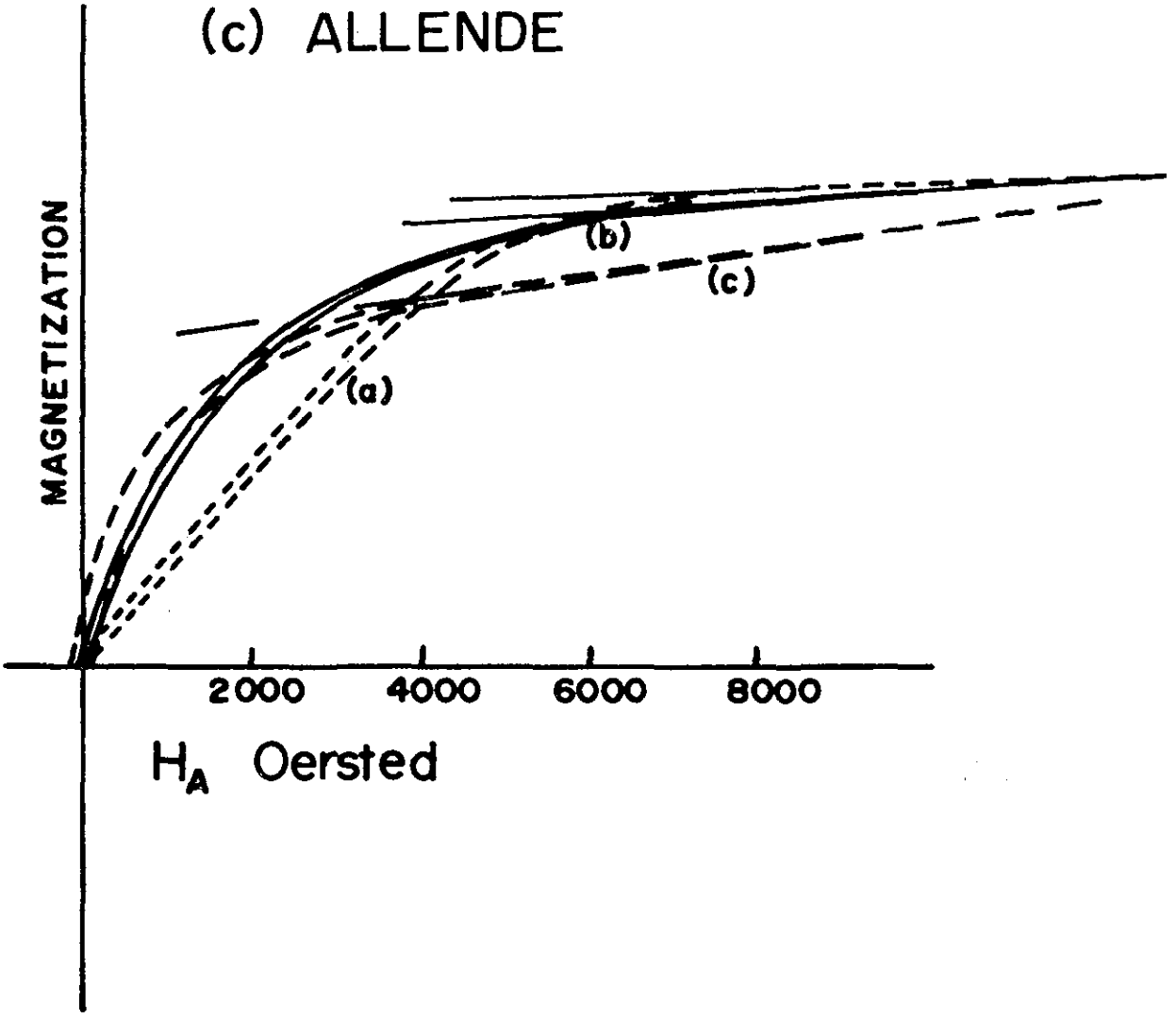
(a) STEEL SPHERE
(b) FOREST CITY
(c) ALLENDE
MAGNETIZATION
(a)
(b)
(c)
2000
4000
6000
8000
H_A Oersted

FIGURE 7

REDUCTION IN COERCIVITY — MIXTURES

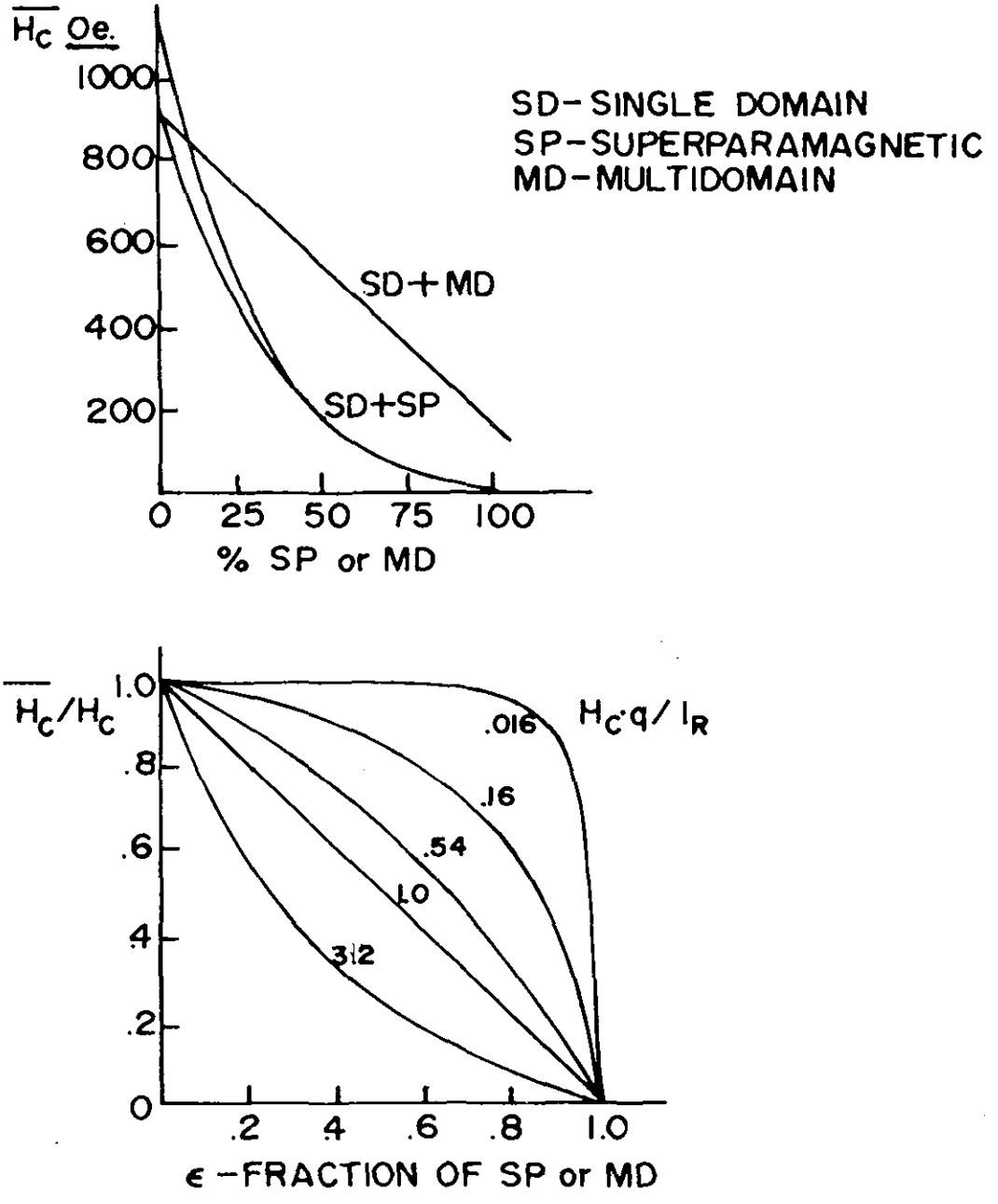

FIGURE 8

EXPERIMENTAL SIMULATION – LOOP CONSTRICTION

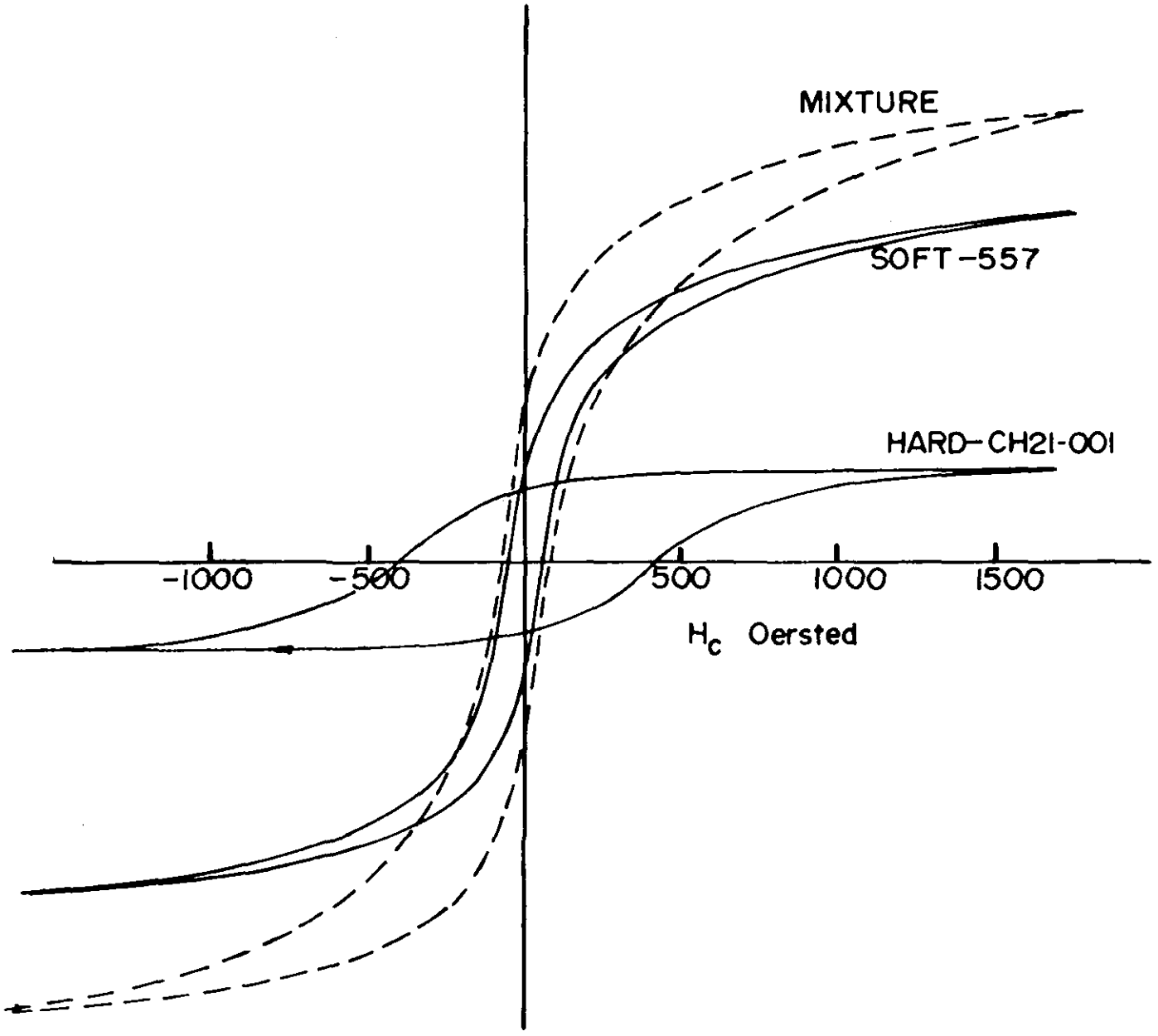

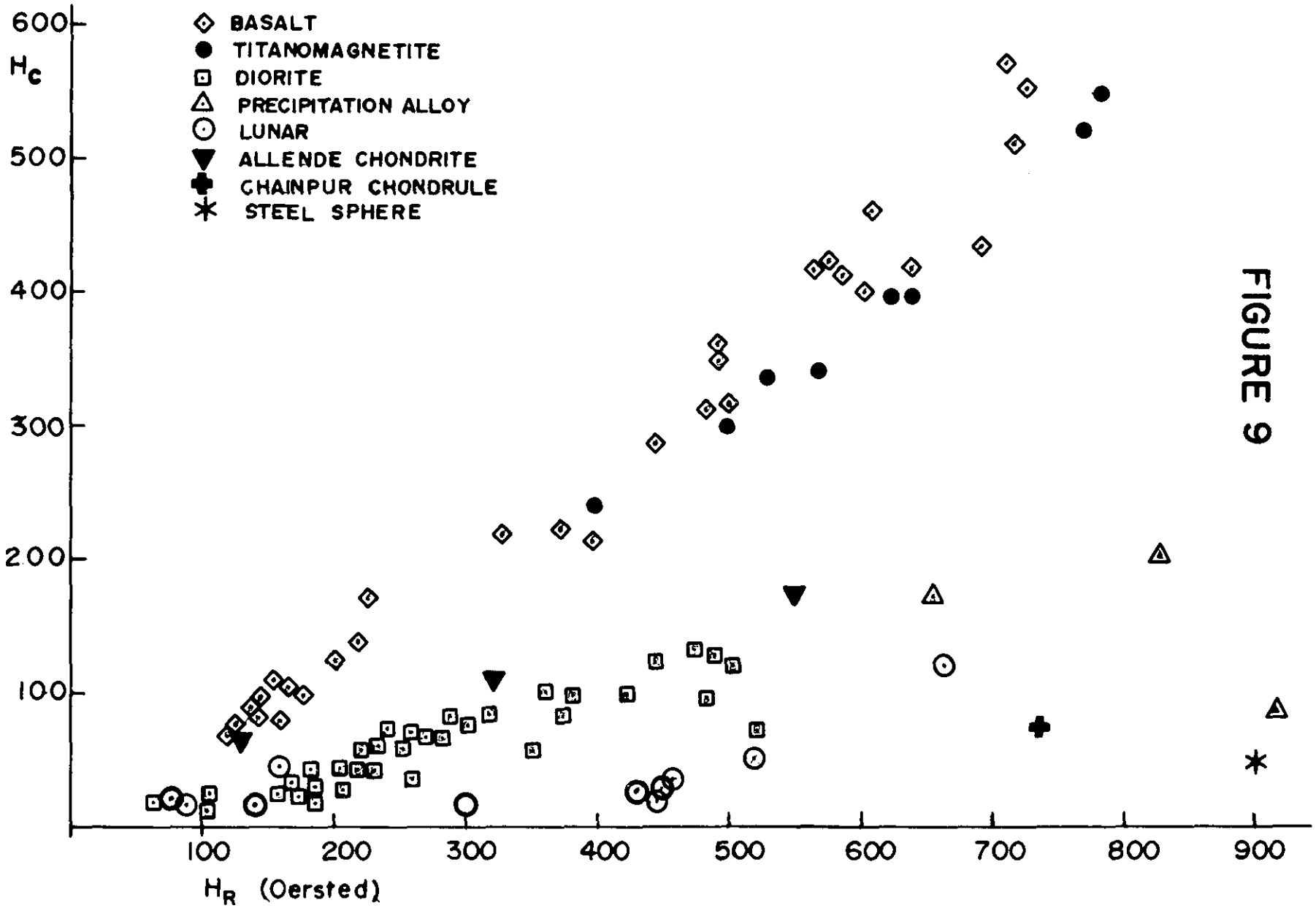
BASALT
TITANOMAGNETITE
DIORITE
PRECIPITATION ALLOY
LUNAR
ALLENDE CHONDRITE
CHAINPUR CHONDRULE
STEEL SPHERE
H_c
600
500
400
300
200
100
100
200
300
400
500
600
700
800
900
H_R (Oersted)

FIGURE 9

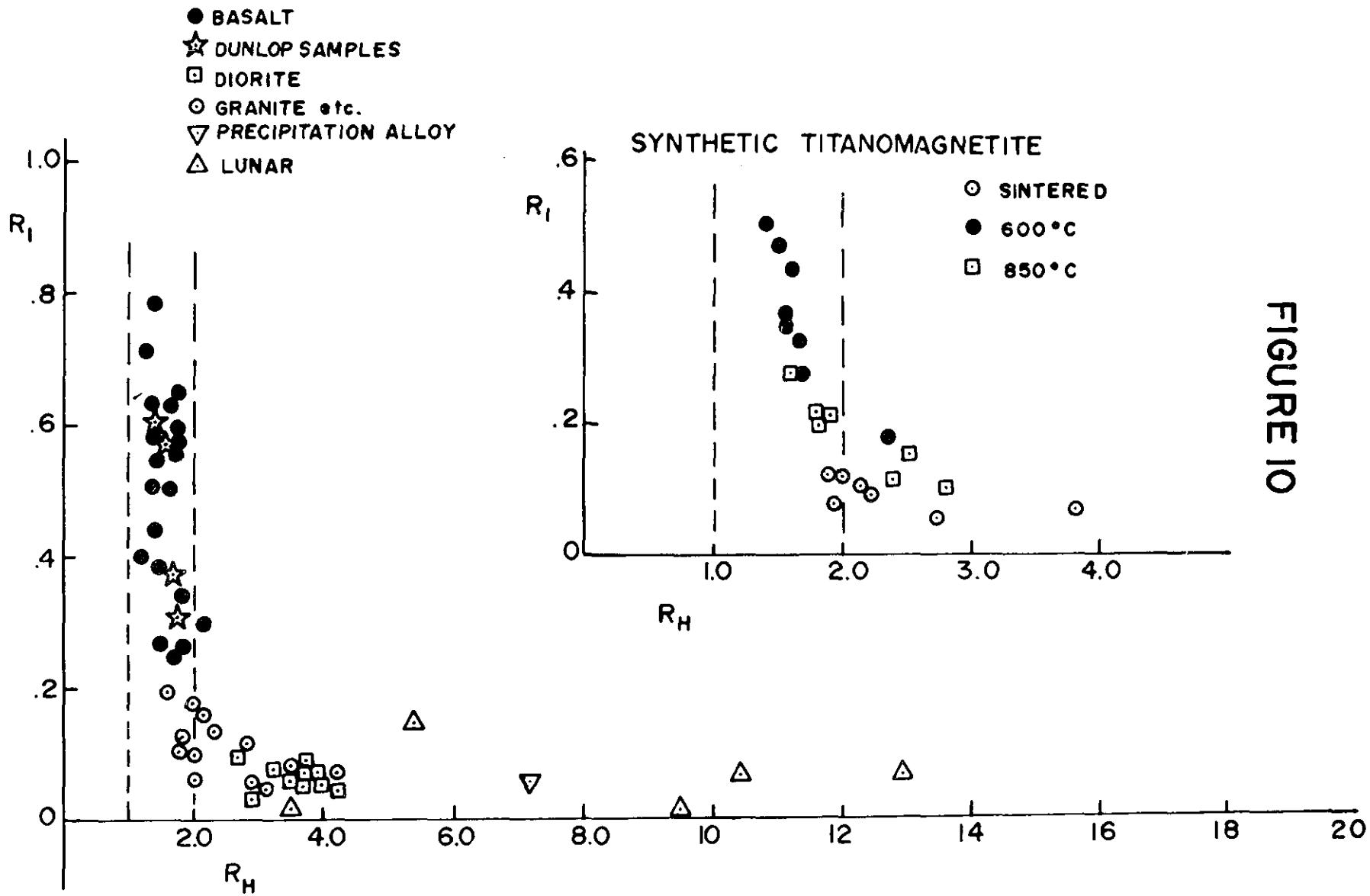
BASALT
DUNLOP SAMPLES
DIORITE
GRANITE etc.
PRECIPITATION ALLOY
LUNAR
R_I
R_H
SYNTHETIC TITANOMAGNETITE
SINTERED
600°C
850°C

FIGURE 10

REFERENCE LIST

Bean, C. P., and I. S. Jacobs, 1960, Magnetization of a dilute suspension of multidomain ferromagnetic: Jour. Appl. Phys., V31, p1228.

Clarke, R. S., E. Jarosewich, B. Mason, J. Nelen, M. Gomez, and J. R. Hyde, 1970, The Allende Mexico meteorite shower: Smithsonian Contrib. Earth Sci. no. 5.

Gaunt, P., 1960, A magnetic study of precipitation in gold-cobalt alloy: Phil. Mag., V5, p1127.

Kneller, E. F., 1969, Fine particle theory in Magnetism and Metallurgy, edited by Berkowitz and Kneller, Acad. Press, Inc., New York.

Kneller, E. F., and F. E. Luborsky, 1963, Particle size dependence of coercivity and remanence of single domain particles: Jour. Appl. Phys., V34, p656.

Lothian, B. W., A. C. Robinson, and W. Sucksmith, 1958, Some magnetic properties of dilute ferromagnetic alloys II: Phil. Mag., V3, p999.

Luborsky, F. E., and T. O. Paine, 1960, Coercive force and remanence of 25 Å to 2000 Å diameter cobalt, iron, and iron cobalt alloy: Four. Appl. Phys., V31, p685.

Luborsky, F. E. and P. F. Lawrence, 1961, Saturation magnetization and size of iron particles less than 100 Å in diameter: Jour. Appl. Phys., V32, p2315.

Meikeljohn, W. H., 1953, Experimental study of the coercive force of fine particles: Rev. Mod. Phys., V25, p302.

Nagata, T., R. M. Fisher, F. C. Schwerer, M. D. Fuller, and J. R. Dunn, 1971, Magnetic properties and remanent magnetization of Apollo 12 lunar materials and Apollo 11 lunar microbreccias: Proc. Second Lunar Science Conf., V3, p2461.

Nagata, T., Y. Ishikawa, H. Kinoshita, M. Kono, Y. Syono, and R. M. Fisher, 1970, Magnetic properties and natural remanent magnetization of lunar materials: Proc. Apollo 11 Lunar Science Conf., V3, p2325.

Parry, L. G., 1965, Magnetic properties of dispersed magnetite powders: Phil. Mag., V2, p303.

Sentfle, F. E., A. N. Thorpe, and R. R. Lewis, 1964, Magnetic properties of nickel-iron spherules from Isabella Phillipine Islands: Jour. Geophys. Res., V69, p317.

Shaw, R. R., and J. H. Heasley, 1967, Superparamagnetic behavior of $MnFe_2O_4$ and Fe_2O_3 precipitated from silicate melts: Jour. Ceram. Soc., V50, p297.

Stoner, E. C., and E. P. Wohlfarth, 1948, A mechanism of magnetic hysteresis in heterogeneous alloys: Phil. Trans. Roy. Soc., V240, p599.

Van Schmus, W. R., and J. A. Wood, 1967, A chemical and petrologic classification for the chondritic meteorites: Geochem. Cosmochim. Acta, V31, p747.

Wasilewski, P. J., 1969, Thermochemical remanent magnetization in basaltic rocks: Experimental characteristics: Jour. Geomag. Geoelec., V21, p595.

Wasilewski, P. J., 1970, Correspondence between magnetic and textural changes in titanomagnetites in basaltic rocks: Thesis, University of Tokyo.

Wasilewski, P. J., 1972a, Magnetic powder technique in rock magnetism research: NASA-Goddard Space Flight Center X Document, X-644-72-164.

Wasilewski, P. J., 1972b, Magnetic hysteresis in natural materials: to be published in Earth Planet. Sci. Lett.

Wasilewski, P. J., 1972c, Particle shape and magnetization of chondrite meteorites, lunar samples, and impactites: NASA-Goddard Space Flight Center, X Document, X-644-72-161.

Wohlfarth, E. P., 1958, Remanent magnetization of fine particles: Jour. Phys. Rad., V20, p295.

Wohlfarth, E. P., 1963, Permanent magnet materials in Magnetism III, edited by Rado and Suhl, Acad. Press, Inc., New York.